**Research paper**                                                                                    **Open Access**

# Preparation of Zinc-Ferrite Nanoparticles and its application for Uranium removal from aqueous Solutions

**Ahmed Said El-Sheikh**

Nuclear Materials Authority, Cairo, El Katameya, Cairo, Egypt.
Email: ahmedshk2003@yahoo.com

**Abstract**

Zinc ferrite nanoparticles ($ZnFe_2O_4$) has been prepared by sol–gel combustion method. Different techniques as SEM, FTIR and EDX techniques were used to characterize the obtained material. The adsorption factors have been optimized. The adsorption capacity of uranium attained 350 mg/g that accords with Langmuir isotherm (357 mg/g). The adsorption process is following pseudo second order reaction. The uranium stripping efficiency from the load Zinc ferrite nanoparticles fulfilled 99.8% at 1 hr. equilibrium time and a phase ratio (S/A) of 0.1 g/10 ml of 1 mol/l $H_2SO_4$.
**Keywords:** Zinc ferrite, nanoparticles, Uranium Adsorption.

## 1. Introduction

Zinc ferrite, a thermally and chemically stable semiconductor material in the range of nanometer scale, shows unexpected behavior both in physical and chemical properties [1]. Zinc ferrite is an appropriate choice for many applications such as photocatalysts [2], gas sensors [3], magnetic resonance imaging [4], actuators [5], pigments [6], and temperature stabilizer over a high-frequency range [7]. Moreover, one of the promising steps to improve the ferrite properties are a substitution of other elements (i.e., cobalt, magnesium, bismuth, copper, etc.) placed in tetrahedral and octahedral sites. Ferrites magnetic properties vary according to the substituted magnetic or non-magnetic materials in its structure. Magnetic spinel ferrites have attracted the researchers due to their extended applications in the fields like magnetic recording, microwave absorbers, water splitting, and biomedical fields [8–11]. In medical field, it is used as magnetic fluid hyperthermia for cancer therapy [12]. Cobalt-substituted zinc ferrites are popularly known as magnetic ceramics. It was adapted in many research fields due to its low core loss, high electrical resistivity, and magnetic softness [13, 14]. Plenty of synthesis techniques are available to synthesize ferrite nanoparticles such as chemical reduction, sol–gel, combustion, co-precipitation, ball milling, micro-emulsion, electro-spinning, polyol route, dip coating, and hydrothermal method. Among them, co-precipitation is very economic and less toxic compared to other techniques [15–24]. Kumar et al. recently investigated the dielectric properties of transition metal-doped spinel ferrites [25]. Hanini et al. synthesized 11 nm sized zinc-ferrite nanoparticles for magnetic hyperthermia therapy applications [26]. Sawant et al. analyzed the comparative study of drug-delivery potentials of surface-functionalized cobalt and zinc-ferrite nanohybrids for curcumin into MCF-7 breast cancer cells [27]. Bhukal investigated the various material substitutions in the Cu–Zn-mixed ferrite to degrade methyl orange [28]. Hochepied and his co-worker elaborately studied the ferromagnetic resonance of non-stoichiometric zinc ferrite and cobalt-dopedzinc-ferrite nanoparticles [29]. Zhang and Raju separately studied the effect of transition metal substitution in the mixed ferrite microstructure and reported the improved magnetic behavior of the spinel ferrites [30,31]. Azadmanjiri investigated the electromagnetic properties of Ni–Zn ferrites prepared by sol–gel combustion method Azadmanjiri investigated the electromagnetic properties of Ni–Zn ferrites prepared by sol–gel combustion method [32]. Sundararajan and his co-workers investigated the photocatalytic degradation of rhodamine B employing zinc-doped cobalt nanoferrites [33]. Fauziatul Fajaroh et. al. synthesized the $ZnFe_2O_4$ nanoparticles by coprecipitation using a PEG (polyethylene glycol) 6000 as a template. It was followed by the performance test of these materials as adsorbents for malachite green which is one of the dyestuffs often used in industry [34]. One of the adsorbent extraction processes after the adsorption process takes place easily when magnetic adsorbents are used, is magnetite nanoparticles. Another advantage of this nano-scale material is its large surface area, so the adsorption capacity is also significant. However, this material has one drawback that is easily oxidized, especially at high temperatures [35]. Therefore, the development of magnetic adsorbents that have high stability is still needed. One of them is the development of zinc ferrite nanoparticles ($ZnFe_2O_4$) which can be used as an adsorbent. The ZnFe2O4 nanoparticles are one of the spinel ferrites which have better chemical and thermal stability [36]. The $ZnFe_2O_4$ nanoparticles can be synthesized by a

hydrothermal method [37], solvothermal [38], and sol-gel [39]. Zaghloul E., et., al., prepared ZnFe$_2$O$_4$ nanoparticles by sol-gel method and used it for the Removing of 2,4-Dichlorophenoxyacetic Acid (2,4-D) from Polluted Water [40]

This paper aims to remove uranium from aqueous solutions. The effects of different parameters such as, pH, dose, contact time, initial concentration on the adsorption efficiency were assessed. The obtained zinc ferrite nanoparticles displayed good activity for removing uranium.

## 2. Experimental

### 2.1. Chemicals and reagents

The standard uranium sulfate solution was prepared by dissolving an appropriate amount of uranyl sulfate trihydrate UO$_2$SO$_4$.3H$_2$O from Ibilabs, Florida, USA. delivered from Sigma Aldrich, Germany. Arsenazo III, ascorbic acid, ammonia solution, ferric nitrate, were obtained from Sigma/Aldrich. Thiourea and zinc nitrate obtained from CarloErba., HCl 37%, HNO$_3$, NaCl and H$_2$SO$_4$ 98% was obtained from Fisher.

### 2.3. Uranium Adsorption Equilibrium Studies from sulfate Solution

The zinc ferrite nanoparticles adsorbent was used for uranium extraction from sulfate solution by batch experiment. In this manner, a fixed weight of zinc ferrite nanoparticles (0.1g) contacted with (10 mL) uranium synthetic solution for known period at ambient temperature. Uranium concentration was measured before and after experiment. The adsorption efficiency was calculated according to relation (1):

$$\text{U adsorption efficiency } \% = \frac{C_o - C_e}{C_o} \times 100$$

……… (1)

Where C$_o$ and C$_e$ are the initial and equilibrium uranium concentration in solution (mg/L), respectively. Calculation of uranium adsorption quantity qe (mg/g) has been carried at the equilibrium time according to relation 2

### 2.2. Preparation of of zinc ferrite nanoparticles

Zinc ferrite powders (ZnFe$_2$O$_4$) were prepared by sol–gel combustion method. Analytical grades of Fe(NO$_3$)$_3$.9H$_2$O, Zn(NO$_3$)$_2$.4H$_2$O and Thiourea (CS (NH$_2$) were used as raw materials. Appropriate amount of nitrates and thiourea (fuel) was first dissolved into deionized water to form a mixed solution with molar ratio of nitrates to thiourea 1:2. pH value of the solution was adjusted to about 9.5 using ammonia solution, then, solution poured into a dish and heated at 70-100 °C under constant stirring to transform into a dried gel. Water removal from the dried gel is a major problem in the sol–gel method, dried gel burnt in a self-propagating combustion way to form loose powder, that performed by heating at 350°C in the oven the transparent solution turned to viscous brown gel followed by foaming of the gel, the combustion reaction was completed within a few seconds and loose powder was formed. The powder crushed and ground thoroughly. The puffy, porous brown powder was calcined at the temperature of 800 °C for 4 h with a heating rate of 10 C/min [41].

$$q_e = (C_o - C_e) \times \frac{V}{m}$$

………… (2)

Where V is the volume of solution (L), m is the weight of the resin (g). The distribution coefficient (K$_d$) of uranium between the aqueous bulk phase and the solid phase was calculated from the following relation (3):

$$K_d = \frac{C_o - C_e}{C_e} \times \frac{V}{m}$$

……………
(3)

### 2.4. Uranium Analysis

Uranium analysis was determined spectrophotometerically using Arzenazo III at 655 nm [42]. In the meantime, this analysis was confirmed by the oxidemetric volumetric determination of uranium using ammonium metavanadate. This procedure is based on the titration of U+4 with ammonium vanadate NH$_4$VO$_3$; namely:

U$^{+4}$ + 2NH$_4$VO$_3$ + 4H$^+$ = UO$_2^{+2}$ + 2VO$^{+2}$ + 2NH$_4^+$ + 2 H$_2$O
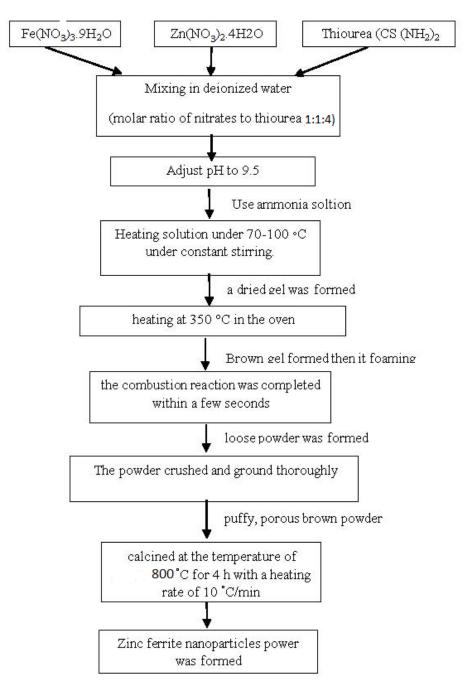
Fig (1): flow chart for zinc ferrite nanoparticles preparation

## 3. Results and Discussion

### 3.1 Uranium adsorption from sulfate solution using zinc ferrite nanoparticles sorbent

The factors that affect the uranium sorption efficiency from sulfate solution using solid-liquid batch technique were studied. The relevant factors include pH, Contact Time, temperature, ZF dose and Initial Uranium Concentration.

### 3.1.1. Effect of pH

The effect of pH on uranium adsorption from zinc ferrite nanoparticles adsorbent from sulfate solution was studied by contacting (0.1g) of zinc ferrite nanoparticles with (10 mL)

uranium synthetic solution of 500 mg/L at room temperature for 3 hrs. The studied pH was ranged from 1.0 to 5.0. The achieved data was presented in Fig. 2. From the obtained results, it could be concluded that the maximum uranium adsorption was achieved at pH between 3.0 and 4.0 was 95 % adsorption efficiency. This is due to the anion complexes of uranium ($UO_2 (SO_4)_2^{2-}$). Accordingly, pH 3.0-4.0 was the best range and consequently, pH 4.0 was selected for the subsequent experiments.
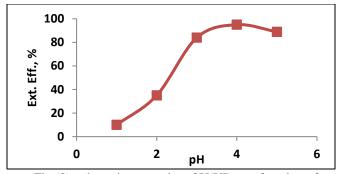
Fig (2): adsorption capacity of U(VI) as a function of equilibrium pH using ZF sorbent
($C_0$: 500 mg/ L; ZF weight = 0.1 g, contact time: 3 hr; T:25 ± 1 ℃)

### 3.1.2. Effect of Equilibrium Time

The adsorption efficiency of Uranium on ZF was examined at different time intervals 0.5–5 hrs and the other conditions were pH 4 ± 0.1, initial uranium concentration of 500 mg/L, dose ratio (0.1g)/ 10 ml uranium solution at room temperature. The results were plotted in Figure 3. It was detected that the uranium adsorption efficiency attained about 82% at 1 hr. By increasing the contact time from 1 to 2 hrs, the adsorption efficiency attained about 93.3%. Then it attained 95% at 3hrs Therefore, 3 hrs. value was selected as the suitable equilibrium time.
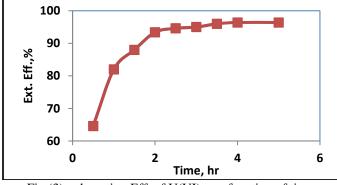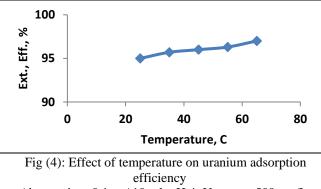


Fig (3): adsorption Eff. of U(VI) as a function of time.
($C_0$: 500 mg L-1; ZF weight = 0.1 g; T:25 ± 1 ℃, pH: 4)

### 3.1.3. Effect of adsorption temperature

The influence of adsorption temperature explored by contacting fixed portions 0.1g of zinc ferrite nanoparticles with 10 ml of 500 mg/L uranium. The other factors were fixed at a contact time of 3hrs, and solution pH of 4.0. Several studies were carried out at a series of temperatures from 25 to 65 °C. The results plotted in Figure 4 showed that, the uranium adsorption efficiency slightly increases with increasing temperature. The increase of uranium sorption at higher temperature may be due to the increase in the activation of the sorbent surface. As the adsorption efficiency was not distinguished, there is no need to control or alter the temperature.



Fig (4): Effect of temperature on uranium adsorption efficiency
(dose ratio = 0.1 g, / 10 ml, pH 4, U conc.= 500 mg/L, contact time, 3 hrs.)

### 3.1.4. Effect of dose ratio (S/L)

The effect of dose concentration has been studied by decreasing the ZF dose from 0.1 to 0.01 g whereas the liquid volume has been stabilized at 10 ml. The other conditions kept at uranium initial concentration of 500 mg/L, pH of 4.0 at ambient temperature for 3 hrs. The result of uranium equilibrium exchange capacity for the zinc ferrite nanoparticles was graphically plotted in figure (5). The results revealed that uranium adsorption efficiency increases gradually by increasing zinc ferrite nanoparticles dose from 0.01 to 0.1 g and stabilized at 0.07 g/10 ml. As a result, zinc ferrite nanoparticles /aqueous ratio of 0.07/10 were the more favorable ratio for the zinc ferrite nanoparticles.
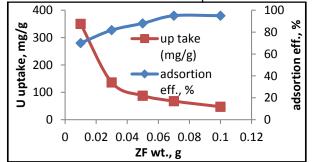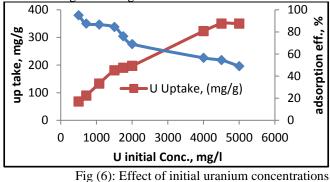


Fig (5): Effect of adsorbent dose upon uranium adsorption efficiency onto ZF (aq. Vol. =10 ml, pH=4, time 3 hr, $C_o$ =500 ppm, 25 ℃ on uranium adsorption efficiency (ZF weight = 0.1 g, volume = 10 ml, pH 4, U conc.= 500 mg/L, contact time, 3 hrs.)

### 3.1.4. Effect of Initial Uranium Concentration

To inspect the effect of initial uranium concentration upon its adsorption efficiency onto ZF, a series of experiments were performed by contacting a fixed weight (0.1 g) of the studied ZF with 10 ml of mg/L uranium stock solution at pH 4 for 3hrs at room temperature (˜25℃). The studied initial uranium concentrations ranged from 500 up to 5000 mg/L. The obtained results were plotted in Figure 6. From the obtained data, it was found that, the adsorption efficiency is inversely proportional to its initial concentration. In contrast, the adsorption capacity is directly proportional to initial uranium concentration till stabilization after 4500

mg/L where at this point experimental adsorption capacity about 350 mg uranium/g ZF.



Fig (6): Effect of initial uranium concentrations on uranium adsorption efficiency and uranium uptake (aq. Solution vol. = 10 ml, pH=4, time 3 hr, ZF wt. = 0.07 g, at 25 $^0$C, pH=4, 3 hrs, 25 $^0$C)

### 3.1.4.1. Adsorption Isotherm

A number of common adsorption isotherm models were considered to fit the attained isotherm data under the equilibrium adsorption of the ZF. Examples of these models are Langmuir and Freundlich.
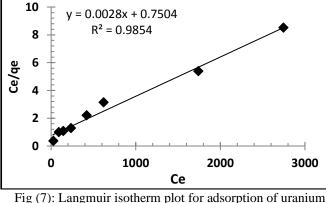
#### A- Langmuir Isotherm

Langmuir model suppose that, the adsorption occurs uniformly on the active sites of the sorbent, and once an asorbate occupies a site, no further sorption can take place at this site [43-45].
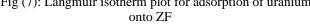
Langmuir model is given by the following equation:

$$\frac{C_e}{q_e}=\frac{C_e}{q_{max}}+\frac{1}{K_L q_{max}} \qquad (4)$$

Where KL is a constant of the adsorption equilibrium (L/mg), qmax is the saturated monolayer adsorption capacity (mg/g) while qe and Ce are the uranium uptake capacity (mg/g) of adsorbent and the residual uranium concentration (mg/L) at equilibrium respectively. A linearized plot of Ce/qe against Ce gives qmax and KL as shown in Figure 7. The Langmuir parameters are given in Table 1. Langmuir model is thus suitable for the description of the adsorption equilibrium of uranium onto material composite.



Fig (7): Langmuir isotherm plot for adsorption of uranium onto ZF

Langmuir model is thus suitable for the description of the adsorption equilibrium of uranium onto material composite.

The essential characteristics of the Langmuir isotherm can be expressed in terms of a dimensionless constant separation factor, $R_L$, which is used to predict if an adsorption system is favorable or not. The separation factor, $R_L$, is given by the following Eq. (5):

$$R_L = \frac{1}{1+K_L C_o} \qquad (5)$$

Where $C_0$ is the initial uranium (VI) concentration (mg/L) and $K_L$ is the Langmuir adsorption constant (L/mg). The calculated $R_L$ value for uranium (VI) concentration of 500 mg U/L is $2.18 \times 10^{-5}$ which was in the range of 0.0 to 1.0 and indicates that the adsorption of uranium (VI) on ZF material is favorable.

#### B- Freundlich Isotherm

The Freundlich model stated that the ratio of solute adsorbed to the solute concentration is a function of the solution. The empirical model was shown to be consistent with exponential distribution of active centers, characteristic of heterogeneous surfaces [42-45]. The amount of solute adsorbed at equilibrium, qe, is related to the concentration of solute in the solution, Ce, by the following:

$$q_e=K_F C_e^{1/n} \qquad (6)$$

This expression can be linearized to give:

$$\log q_e=\log K_F+\frac{1}{n}\log C_e \qquad (7)$$

Where $K_F$ and n are the Freundlich constants, which represent adsorption capacity and adsorption intensity, respectively. A plot of ($\log q_e$) versus ($\log C_e$) results in a straight line with a slope of ($1/n$) and intercept of ($\log K_F$) as seen in Figure (8). Freundlich constants are given in Table 1.
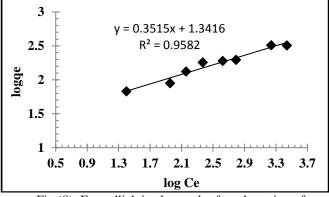


Fig (8): Freundlich isotherm plot for adsorption of uranium onto ZF

Table (1): Langmuir and Freundlich parameters for uranium adsorption onto ZF

| Langmuir model parameters | | | Freundlich model parameters | | |
|---|---|---|---|---|---|
| $q_{max}$, (mg/g) | $K_L$, | $R^2$ | $K_f$ (mg/g) | n | $R^2$ |
| 357 | 1.08 | 0.9854 | 22 | 2.844 | 0.9582 |

By comparing the isotherms applied with the experimental results, Langmuir gave the best fit, while Freundlich isotherm did not fit well.

### 3.1.6. Adsorption Kinetics and Mechanism

The data obtained from batch experiments which were performed at different temperatures (25–65) $^0$C were evaluated by using the simple Lagergren equation [46] to determine the rate of the sorptive interactions assuming pseudo first order kinetics. Thus, the Langmuir model is given by the relation (8):

$$Log\,(q_e - q_t) = Logq_e - \left(\frac{K_1}{2.303}\right)t \quad \cdots\cdots \quad (8)$$

Where $q_t$ and $q_e$ are the amounts of uranium adsorbed (mg/g) at time, t (min) and equilibrium time (3 hrs), respectively and $K_1$ is the pseudo first order Lagergren adsorption rate constant (min $^{-1}$). The $K_1$ values could be obtained by plotting log (qe – qt) versus t for adsorption of uranium at different temperatures as shown in Figure 9. The values of $K_1$ indicate that the rate of the process increases with temperature. The first order mechanism suffered from inadequacies when applied to uranium adsorption on the ZF. The experimental qe values differed from the corresponding theoretical values. Thus, the interaction of uranium with the ZF does not follow the first order kinetics.
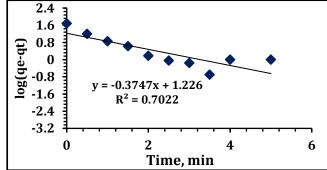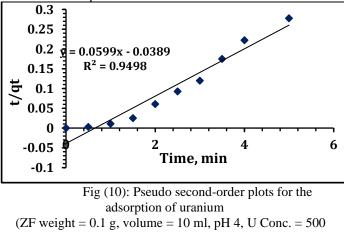


$$y = -0.3747x + 1.226$$
$$R^2 = 0.7022$$

Fig (9): Lagergren plots for the adsorption of uranium (ZF weight = 0.1 g, volume= 10 ml, pH 4, U Conc. = 500 mg/L)

In order to ensure the description of the kinetics, second order kinetic equation was applied which can be represented by the following linear equation [47]:

$$\frac{t}{q_t} = \frac{1}{K_2 q_e^2} + \left(\frac{1}{q_e}\right)t \quad \cdots\cdots \quad (9)$$

Where $K_2$ is the second order rate constant (g. mg-1 min-1). The kinetic plots of t/qt versus t for uranium are shown in Figure 10. The plots show straight lines with good linearity temperatures. For the pseudo second order kinetic model, the correlation coefficients are closer to unity. The calculated equilibrium adsorption capacity (qe) is matches with the experimental data. The $K_2$ values show the applicability of the above equation for the ZF. Therefore, the adsorption reaction is following the pseudo second order sorption more favorable as the predominant mechanism.



$$y = 0.0599x - 0.0389$$
$$R^2 = 0.9498$$

Fig (10): Pseudo second-order plots for the adsorption of uranium
(ZF weight = 0.1 g, volume = 10 ml, pH 4, U Conc. = 500 mg/L)

Table (2): Data of kinetic parameters for uranium adsorption onto ZNF

| Temp, $^oC$ | Lagergren pseudo first-order | | | | pseudo second-order | | | |
|---|---|---|---|---|---|---|---|---|
| | $K_1$ (min $^{-1}$) | $q_{ecal}$ (mg/ g) | $q_{eexp}$ (mg/ g) | $R^2$ | $K_2$ (min $^{-1}$) | $qe_{cal}$ (mg/ g) | $qe_{exp}$ (mg/ g) | $R^2$ |
| 25 | 1.45 | 16.8 | 350 | 0.7022 | 0.00389 | 257 | 350 | 0.9498 |

### 3.1.5. Characterization of Zinc Ferrite Nanoparticles
### 3.1.5.1. Fourier Transform Infrared (FTIR)

The FTIR study of synthesized nano crystal zinc ferrite nanoparticle was performed using Frontier FTIR (Bruker Optics). The FTIR spectra as shown in Fig. 11 confirm the formation of spinel structure. The FTIR spectra of spinel ferrites show two high frequency absorption bands 447and 559cm-1 due to tetrahedral and octahedral M-O stretching vibration respectively. The presence of humidity in prepared samples is shown in FTIR spectra. The bond around 16 29 cm-1 and 34 34cm-1 are due to moisture (O-H group) in samples [48]. This results also in agreement with the results obtained by Sivakumar et. al., [49].
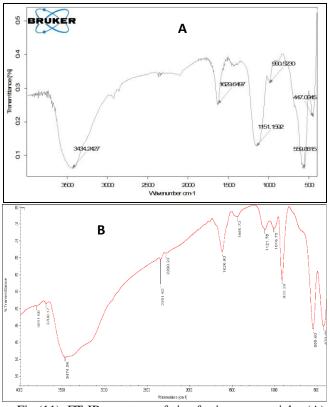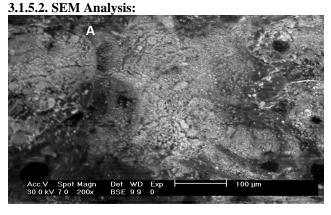
Fig (11): FT-IR spectrum of zinc ferrite nanoparticles (A) before and (B) after uranium adsorption
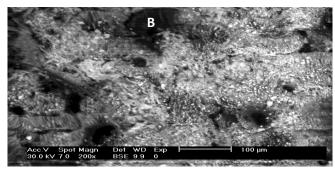
### 3.1.5.2. SEM Analysis:





Fig (12): SEM analysis of zinc ferrite nanoparticles before (a) and after (B) U loading

The SEM images of the Zn-ferrite sample as shown in Figure (12) indicated that the morphology of particles were almost spherical, regular in shape and dispersed uniformly, but agglomerated to some extent due to the interaction between the magnetic nanoparticles, whereas the gel exhibits a relatively porous network. This results in agreement with that revealed by Sivakumar et. al.,[49].



Fig (13): EDX analysis of zinc ferrite nanoparticles before (a) and after (b) U adsorption

Table (3): Quantification results of EDX analysis of zinc ferrite nanoparticles before and after U adsorption

| Before adsorption | | After adsorption | |
|---|---|---|---|
| Element | Wt. % | Element | Wt. % |
| S | 5.11 | S | 1.75 |
| Ca | 3.65 | Ca | 2.22 |
| Fe | 44.39 | Fe | 17.22 |
| Ni | 4.11 | Ni | 3.27 |
| Zn | 42.74 | Zn | 11.38 |
| | | U | 64.17 |
| Total | 100 | | 100 |

### 3.2. Uranium Elution

In order to achieve good metal elution form the nano composite, a number of stripping testes were carried out to elute the uranium ion from the loaded zinc ferrite nanoparticles after sorption process by using different solutions such as HCl, $H_2SO_4$, $HNO_3$ and NaCl, to obtain the maximum stripping percent. Metal stripping experiments were performed using batch method at room temperature. The stripping experiments were carried out by shaking 0.1g loaded ZF and 10 ml of 1 molar for eluting reagent for 1 hour at 250 rpm. The result of uranium stripping from the composite material by using different solution was graphically plotted in figure (14). From the obtained result, it is clearly obvious that, $H_2SO_4$ is the best eluent with 99.8 % stripping efficiency.
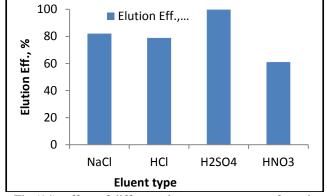


Fig (14): effect of different eluents on recovery of uranium

**Case Study**

The studied optimum conditions have been applied to real technological sample (nuclear waste mixture from the Nuclear Materials Authority) assay 148 ppm uranium and its chemical composition are shown in table 3. By applying the obtained conditions, we found that the adsorption capacity was found to be 93.4% of the theoretical capacity that was realized under the working conditions. The decrease in the ZF capacity after contacting with the nuclear waste mixture

sample may be due to the competition between uranium and ions present in the waste sample.

Table (4) Chemical composition of the studied nuclear waste mixture

| Element | Conc., mg/l |
|---------|-------------|
| U | 148 |
| Ca | 212 |
| Fe | 53 |
| Mg | 118 |
| Zn | 15 |
| Ni | 45 |
| La | 86 |

### 4. Conclusion

The batch tests which were performed to optimize the uranium adsorption by ZF indicate that 350 mg U/g ZF maximum saturation capacity was attained by adjusting the pH at 4 for 3 hrs. contact time and with ZF to Liquor ratio of 0.07/10 at ambient temperature.

The adsorption reaction was found to be more favorably to be pseudo-second order adsorption (Lagergren equation), this is due to that the predominate mechanism and the values of $K_2$ "second order rate constant" indicate that the rate of the process decreases with increasing temperature. Langmuir isotherm model is suitable for the description of the adsorption equilibrium of uranium onto ZF. Uranium elusion has been achieved with 99.8 elusion efficiency by using 1 M $H_2SO_4$. A case study has been applied for a technological sample from Egyptian nuclear materials authority and achieved 93.3% uranium adsorption efficiency.

### References

[1] L.R. Gonsalves, S.C. Mojumdar, V.M.S. Verenkar, Synthesis and characterization of $Co_{0.8}Zn_{0.2}Fe_2O_4$ nanoparticles. J. Therm. Anal. Calor. 104 (2011) 869–873.

[2] A. Manikandan, J.J. Vijaya, M. Sundararajan, C. Meganathan,L.J. Kennedy, M. Bououdina, Optical and magnetic properties $Zn0.02Fe_2O_4$of Mg-doped $ZnFe_2O$ nanoparticles prepared by rapid microwave combustion method.Superlattices Microstruct. 64 (2013)118–131.

[3] P. Rao, R.V. Godbole, S. Bhagwat, Copper doped nickel ferrite nano-crystalline thin films: a potential gas sensor towards reducing gases.Mater.Chem.Phys.171 (2016) 260–266.

[4] C.S. Hwang, N.C. Wang, Preparation and characteristics of ferrite catalysts for reduction of $CO_2$., Mater. Chem. Phys. 88 (2004) 258–263.

[5] N. Somaiah, T.V. Jayaraman, P.A. Joy, D. Das, Magnetic and magnetoelastic properties of Zn-doped cobalt-ferrites-$CoFe2-x$ $Znx$ $O_4(x = 0, 0.1, 0.2, and 0.3)$. J. Magn. Magn. Mater. 324 (2012) 2286–2291.

[6] R.M. Sebastian, K. Maniammal, S. Xavier, E.M. Mohammed, Structural and dielectric studies of $Cr^{3+}$ doped $ZnFe_2O_4$, nanoparticles NanoStud. 8 (2013) 121–130.

[7] G. Kogias, V.T. Zaspalis, Temperature stable MnZn ferrites for applications in the frequency region of 500 kHz. Ceram. Int. 42 (2016) 7639–7646.

[8] A.M. Abu-Dief, M.S.M. Abdelbaky, D. Martínez-Blanco, Z.Amghouz, S. Garcia-Granda, Effect of chromium substitution on the structural and magnetic

properties of nanocrystalline zinc ferrite. Mater. Chem. Phys.174 (2016) 164–171.

[9] S. Salman, S. Afghahi, M. Jafarian, Y. Atassi, C.A. Stergiou, Single and double layer composite microwave absorbers with hexa ferrite BaZn0.6Zr0.3X0.3Fe10.8O (X = Ti, Ce, Sn). Mater. Chem. Phys. 186 (2017) 584–591.

[10] W.M. Shaheen, Effects of thermal treatment and doping with cobalt and manganese oxides on surface and catalytic properties of ferric oxide. Mater. Chem. Phys. 101 (2007) 182–190.

[11] A.K. Gupta, M. Gupta, Synthesis and surface engineering of iron oxide nanoparticles for biomedical applications. Biomaterials. 26 (2005) 3995–4021.

[12] P. Chandrasekharan, D. Maity, C.X. Yong, K.H. Chuang, J. Ding,S.S. Feng, Vitamin E (d-alpha-tocopheryl-co-poly (ethylene glycol) 1000 succinate) micelles-superparamagnetic iron oxide nanoparticles for enhanced thermotherapy and MRI. Biomaterials.32 (2011) 5663–5672.

[13] W. Fu, S. Liu, W. Fan, H. Yang, X. Pang, J. Xu, G. Zou, Hollow glass microspheres coated with $CoFe_2O_4$ and its microwave absorption property. J. Magn. Magn. Mater. 316 (2007) 54–58.

[14] E. Manova, B. Kunev, D. Paneva, I. Mitov, L. Petrov, Mechano synthesis, characterization, and magnetic properties of nanoparticles of cobalt ferrite, $CoFe_2O_4$. Chem. Mater. 16 (2004) 56-89.

[15] N.A.S. Nogueira, V.H.S. Utuni, Y.C. Silva, P.K. Kiyohara, I.F. Vasconcelos, M.A.R. Miranda, J.M. Sasaki, X-ray diffraction and Mossbauer studies on superparamagnetic nickel ferrite ($NiFe_2O_4$) obtained by the proteic sol–gel method. Mater. Chem. Phys. 163 (2015) 402–406.

[16] M.U. Islam, F. Aen, S.B. Niazi, M. Azhar Khan, M. Ishaque,T. Abbas, M.U. Rana, Electrical transport properties of CoZn ferrite–SiO composites prepared by co-precipitation technique.Mater. Chem. Phys. 109 (2008) 482–487.

[17] Z.H. Yang, Z.W. Li, Y.H. Yang, Structural and magnetic properties of plate-like W-type barium ferrites synthesized with a combination method of molten salt and sol–gel. Mater. Chem.Phys. 144 (2014) 568–574.

[18] U. Kurtan, H. Erdemi, A. Baykal, H. Gungunes, Synthesis and magneto-electrical properties of $MFe_2O_4$ (Co, Zn) nanoparticles by oleylamine route. Ceram. Int. 42 (2016) 13350–13358.

[19]. J. Topfer, A. Angermann, Nanocrystalline magnetite and Mn–Zn ferrite particles via the polyol process: synthesis and magnetic properties. Mater. Chem. Phys. 129 (2011) 337–342.

[20] S. Bid, S.K. Pradhan, Preparation of zinc ferrite by high-energy ball-milling and microstructure characterization by Rietveld's analysis. Mater. Chem. Phys. 82 (2003) 27–37.

[21] J. Rehman, M. Azhar Khan, A. Hussain, F. Iqbal, I. Shakir, G.Murtaza, M. Niaz Akhtar, G. Nasar, M. Farooq

Warsi, Structural, magnetic and dielectric properties of terbium doped NiCoX strontium Hexagonal nano-ferrites synthesized via micro-emulsion route. Ceram. Int. 42 (2016) 9079–9085.

[22]. S.J. Azhagushanmugam, N. Suriyanarayanan, R. Jayaprakash, Magnetic properties of zinc-substituted cobalt ferric oxide nanoparticles: correlation with annealing temperature and particle size.Mater. Sci. Semicond. Process. 21 (2014) 33–37.

[23] A. Schutz, M. Gunthner, G. Motz, O. Greibl, U. Glatzel, High temperature (salt melt) corrosion tests with ceramic-coated steel. Mater. Chem. Phys. 159 (2015) 10–18.

[24] H. Yang, X. Zhang, G. Qiu, Formation of $NiFe_2O_4$ nanoparticles by mechanochemical reaction. Mater. Res. Bull. 39 (2004) 833-837.

[25] A. Kumar, P. Sharma, D. Varshney, Structural, vibrational and dielectric study of Ni doped spinel Co ferrites:  $Co1-xNi_xFe_2O_4$(x = 0.0, 0.5, 1. Ceram. Int. 40(8) (2014) 12855–12860.

[26] L. Hanini, J. Lartigue, K. Gavard, C. Kacem, F. Wilhelm, F.Gazeau, S. Chau, Ammar, Zinc substituted ferrite nanoparticles with  $Zn_{0.9}Fe_{2.1}O_4$ formula used as heating agents for in vitro hyperthermia assay on glioma cells. J. Magn. Magn. Mater. 416 (2016) 315–320.

[27] V.J. Sawant, S.R. Bamane, R.V. Shejwal, S.B. Patil, Comparison of drug delivery potentials of surface functionalized cobalt and zinc ferrite nanohybrids for curcumin in to MCF-7 breast cancer cells, J. Magn. Magn. Mater. 417 (2016) 222–229.

[28] S. Bhukal, M. Dhiman, S. Bansal, M.K. Tripathid, S. Singhal,Substituted Co–Cu–Zn nanoferrites: synthesis, fundamental andredox catalytic properties for the degradation of methyl orangRSC Adv. 6 (2016) 1360–1375.

[29] J.F. Hochepied, M.P. Pileni, Ferromagnetic resonance of nonstchiometric zinc ferrite and cobalt-doped zinc ferrite nanoparticles.J. Magn. Magn. Mater. 231(2001) 45–52.

[30] C.F. Zhang, X.C. Zhong, H.Y. Yu, Z.W. Liu, D.C. Zeng, Effects of cobalt doping on the microstructure and magnetic properties of Mn–Zn ferrites prepared by the co-precipitation method. Phys.B 404 (2009) 2327–2331.

[31] K. Raju, G. Venkataiah, D.H. Yoon, Effect of Zn substitution on the structural and magnetic properties of Ni–Co ferrites. Ceram.Inter. 40 (2014) 9337–9344.

[32] J. Azadmanjiri, Structural and electromagnetic properties of Ni–Zn ferrites prepared by sol–gel combustion method. Mater. Chem. Phys. 109 (2008) 109–112.

[33]. M. Sundararajan, V. Sailaja, L.J. Kennedy, J.J. Vijaya, Photocatalytic degradation of rhodamine B under visible light using nanostructured zinc doped cobalt ferrite: kinetics and mechanism. Ceram.Int.43 (2017) 540–548.

[34] Fauziatul Fajaroh, Ita Desi Susilowati, Nazriati, Sumari, Adrian Nur, Synthesis of $ZnFe_2O_4$ Nanoparticles with PEG 6000 and Their Potential Application for Adsorbent. IOP Conf. Series: Materials Science and Engineering 515 (2019) 012049.

[35] R. M. Cornell and U. Schwertmann, The Iron Oxides (Weinheim, FRG: Wiley-VCH Verlag GmbH & Co. KGaA (2003) ISBN 3-527- 30274-3.

[36] R. Voda, A. Negrea, L. Lupa, M. Ciopec, P. Negrea, C. M. Davidescu , M. Butnariu, Nanocrystalline ferrites used as adsorbent in the treatment process of waste waters resulted from ink jet cartridges manufacturing Open Chemistry 13 (2015) 743-747.

[37] M. M. A. Sinthiya, K. Ramamurthi, S. Mathuri, T. Manimozhi, N. Kumaresan, M. M. Margoni, P. C. Karthika, Synthesis of Zinc Ferrite ($ZnFe_2O_4$) Nanoparticles with Different Capping Agents. Int. J. Chem. Tech. Res. 7 (2015) 2144-2149.

[38] V. Blanco-Gutiérrez, M. J. Torralvo, R. Sáez-Puche and P. Bonville, Magnetic properties of solvothermally synthesized $ZnFe_2O_4$ nanoparticles Journal of Physics: Conference Series (2010) 200072013.

[39] F. Iqbal, M. I. A. Mutalib, M. S., Shaharun, M. khan and B. Abdullah, Synthesis of $ZnFe_2O_4$ Using sol-gel Method: Effect of Different Calcination Parameters. Procedia Engineering 148 (2016) 787–794.

[40] E. Zaghloul, A. Amin, M. Diab, A., Elsonbati, M. Ibrahim, Removing 2,4-Dichlorophenoxyacetic Acid (2,4-D) from Polluted Water using Zinc Ferrite Nanoparticles. Egypt.J.Chem. 63, (2020) No. 6.

[41] S. Khorrami, F. Gharib, G. Mahmoudzadeh, S. Sadat Sepehr, S. Sadat Madani, N. Naderfar, S. Manie, Synthesis and characterization of nanocrystalline spinel Zinc ferrite prepared by sol-gel auto-combustion technique. International Journal of Nano Dimension, 1(3) (2011) 221-224.

[42] Z. Marczenko, Spectrophotometric Determination of the Elements, John Wily, London. (1976).

[43] I. Langmuir, J. Am. Chem. Soc. 38 (1916) 2221–2295.

[44] M.F. Freundlich, Z. Phys. Chem. 57 (1996) 385–470.

[45] M. Manes, L.J.E. Hofer, Application of the Polanyi adsorption potential theory to adsorption from solution on activated carbon, The Journal of Physical Chemistry 73(3) (1969) 584–590.

[46] S. Lagergren, Zur theorie der sogenannten adsorption gelo ̈ster stoffe Kungliga venska Vetenskapsakademiens. Handlingar. 24 (4) (1898) 1–39.

[47] Y.S. Ho, G. McKay, Pseudo-second order model for sorption processes. Process Biochem. 34 (1999) 451- 465.

[48] A. Hajalilou, E. Abouzari-Lotf, V. Abbasi-Chianeh, T. R. Shojaei, E. Rezaie, Inclusion of octahedron-shaped ZnFe2O4 nanoparticles in combination with carbon dots into carbonyl iron based magnetoheological suspension as additive. J alloys Compd. 737 (2018) 536-548.

[49] P. Sivakumar, K. Thyagarajan, A. G. Kumar, Investigations on physical properties of Zn ferrite nanoparticles using sol-gel auto combustion technique. Dig. J. Nanomater Biostruct, 13(4) (2018) 1117-1122.